

Lattice BGK Model for Incompressible Axisymmetric Flows

Ting Zhang¹, Baochang Shi^{2,*}, Zhenhua Chai² and Fumei Rong¹

¹ State Key Laboratory of Coal Combustion, Huazhong University of Science and Technology, Wuhan 430074, China.

² School of Mathematics and Statistics, Huazhong University of Science and Technology, Wuhan 430074, China.

Received 29 August 2010; Accepted (in revised version) 5 August 2011

Communicated by Kazuo Aoki

Available online 3 January 2012

Abstract. In this paper, a lattice Boltzmann BGK (LBGK) model is proposed for simulating incompressible axisymmetric flows. Unlike other existing axisymmetric lattice Boltzmann models, the present LBGK model can eliminate the compressible effects only with the small Mach number limit. Furthermore the source terms of the model are simple and contain no velocity gradients. Through the Chapman-Enskog expansion, the macroscopic equations for incompressible axisymmetric flows can be exactly recovered from the present LBGK model. Numerical simulations of the Hagen-Poiseuille flow, the pulsatile Womersley flow, the flow over a sphere, and the swirling flow in a closed cylindrical cavity are performed. The results agree well with the analytic solutions and the existing numerical or experimental data reported in some previous studies.

PACS: 47.11-j, 02.60.Cb

Key words: Lattice BGK model, incompressible axisymmetric.

1 Introduction

In the past few years, the lattice Boltzmann methods (LBM) originated from kinetic theory, have gained much attention in hydrodynamics [1–5]. Compared with the traditional methods (for example, finite difference method, finite element method and finite volume method), the LBM have many advantages, such as the simplicity of program, location of computation, nature parallelism and easiness in dealing with complex boundary. The

*Corresponding author. *Email addresses:* zting198525@hotmail.com (T. Zhang), sbchust@126.com (B. Shi), hustczh@126.com (Z. Chai), rongfmhust@gmail.com (F. Rong)

lattice BGK (LBGK) model, as the most popular LBM, has been successfully applied to study a variety of fields such as flow in porous media, heat transfer, turbulence, blood flow, Chemical reactions, and multiphase and multicomponent flows. It is well known that when the standard LBGK model is used to simulate incompressible fluid flows, there may be compressible effects existed which might lead to some undesirable errors. In order to eliminate the compressible effects, many authors have developed some incompressible LBGK models [6–10]. Only Guo's LBGK model [10] can effectively eliminate the compressible effect induced by density variation, and the incompressible Navier-Stokes (NS) equations can be exactly recovered from this model.

Up to now, there are some LBGK models proposed for axisymmetric flows. To simulate the three-dimensional (3D) axisymmetric flows on the Cartesian coordinate system [11–13], the most direct way is to apply certain 3D LBGK models with suitable curved boundary treatment. However, it is well known that 3D axisymmetric flows are in effect 2D problem in the cylindrical coordinate system. In order to make use of the advantages of the axisymmetric properties, Halliday et al. firstly developed the LBGK model for axisymmetric flows [14]. They inserted "source" or "forcing" terms into the evolving equations so that it could recover the axisymmetric Navier-Stokes (NS) equations. Shortly after the presentation of this method, Premnath and Mukherjee extended it to multiphase flows and two-phase flows with larger density ratio respectively [15, 16]. Unfortunately, the model of Halliday et al. was found to miss some important terms relative to the radial velocity. Additionally, since this model was derived from the standard LBGK model, the compressible effect can not be eliminated. Lee et al. [17] firstly point out these limitations and developed a more accurate axisymmetric LBGK model from the incompressible LBGK model proposed by He and Luo [9]. Shortly afterwards, Reis and Phillips developed a modified model following the philosophy proposed by Halliday [18, 19]. Zhou presented a much simpler axisymmetric LBGK model in the year 2008 [20]. Through Chapman-Enskog (C-E) expansion, the added source terms in the model happened to be the additional in the governing equations for the axisymmetric flows compared with the NS equations. Recently, Chen et al. developed an incompressible D2Q5 LBGK model for axisymmetric flows based on the vorticity-stream equations [21].

Although the above axisymmetric LBGK models have been used to simulate various flows [22–30], they still have some limitations. Firstly as pointed out in [31], these models (except for the one in [21]) almost include many velocity gradients in the source terms. The discretization of these gradient terms may leads to additional errors and numerical instability. Although the model in [21] can simplify the source terms, a Poisson equation must be solved at each time step will lead to inefficient for unsteady flows. Secondly, all of these models neglect the azimuthal velocity. Finally, most of these models (except the ones in [17] and [21]) are constructed from the standard LBGK model, so they can only be viewed as artificial compressible methods for simulating incompressible axisymmetric flows. When the model proposed in [17] is used to simulate unsteady incompressible axisymmetric flows, in order to neglect the artificial compressible effect, an additional conditions, $L_x/(TC_s) \ll 1$, must be required. Furthermore, the average pressure of the

flow must be specified in advance, but in practice, the average pressure is not known or can not be prescribed precisely.

Recently, Guo et al. proposed a more effective axisymmetric LBGK model based on the axisymmetric Boltzmann equation [31]. This model contained no velocity gradients in the source terms, so it is much simpler than the existing models. Additionally, the model can describe the velocities in all directions and therefore is complete. Recently, Wang et al. extended the model to multi-relaxation-time lattice Boltzmann model (MRT-LBM) [32]. However, the compressible effect also exists in these axisymmetric models.

In this paper, a simple LBGK model for the incompressible axisymmetric flows is proposed. The model can eliminate the compressible effects only with the small Mach number limit and has no velocity gradients in source terms. Furthermore, the model also can describe the azimuthal velocity. The rest of the paper is organized as follows. In Section 2 an incompressible LBGK model for axisymmetric flows is designed. Boundary conditions and force evaluation methods are described in Section 3. Numerical results are performed in Section 4 to test the incompressible axisymmetric LBGK model. Finally, Section 5 summarizes the results and concludes the paper.

2 Incompressible axisymmetric LBGK model

2.1 Incompressible axisymmetric Navier-Stokes equations

The governing equations for the incompressible axisymmetric flows in the cylindrical coordinate system (x, r, θ) can be written as [31]

$$\frac{\partial u_x}{\partial x} + \frac{1}{r} \frac{\partial(ru_r)}{\partial r} = 0, \quad (2.1a)$$

$$\rho \frac{du_x}{dt} = -\frac{\partial p}{\partial x} + \mu \left[\frac{1}{r} \frac{\partial}{\partial r} \left(r \frac{\partial u_x}{\partial r} \right) + \frac{\partial^2 u_x}{\partial x^2} \right] + \rho a_x, \quad (2.1b)$$

$$\rho \frac{du_r}{dt} = -\frac{\partial p}{\partial r} + \mu \left[\frac{\partial}{\partial r} \left(\frac{1}{r} \frac{\partial(ru_r)}{\partial r} \right) + \frac{\partial^2 u_r}{\partial x^2} \right] + \rho \frac{u_\theta^2}{r} + \rho a_r, \quad (2.1c)$$

$$\rho \frac{du_\theta}{dt} = \mu \left[\frac{\partial}{\partial r} \left(\frac{1}{r} \frac{\partial(ru_\theta)}{\partial r} \right) + \frac{\partial^2 u_\theta}{\partial x^2} \right] - \rho \frac{u_\theta u_r}{r} + \rho a_\theta, \quad (2.1d)$$

where

$$\frac{d\phi}{dt} = \frac{\partial\phi}{\partial t} + \frac{\partial(u_x\phi)}{\partial x} + \frac{1}{r} \frac{\partial(ru_r\phi)}{\partial r},$$

for any variable ϕ . Here x , r , and θ are the coordinates in axial, radial, and azimuthal directions, respectively, ρ is the density with $\rho \approx \text{const}$, p is the pressure, t is the time, u_i is the component of velocity in the i direction. $\vec{F} = \rho \mathbf{a} \equiv \rho(a_x, a_r, a_\theta)$ is the external force.

Based on the idea in Guo's axisymmetric LBGK model [31], we rewrite Eq. (2.1) through multiplying Eqs. (2.1a)-(2.1c) with r and Eq. (2.1d) with r^2 , and dividing by ρ

on both sides

$$\nabla \cdot (r\mathbf{u}) = 0, \quad (2.2a)$$

$$\frac{\partial(r\mathbf{u})}{\partial t} + \nabla \cdot (r\mathbf{u}\mathbf{u}) = -\nabla(P_r) + \nu \nabla^2(r\mathbf{u}) - \nu \frac{\partial \mathbf{u}}{\partial r} + \mathbf{H} + \mathbf{F}, \quad (2.2b)$$

$$\frac{\partial(r^2 u_\theta)}{\partial t} + \nabla \cdot (r^2 \mathbf{u} u_\theta) = \nu \nabla^2(r^2 u_\theta) - 3\nu \frac{\partial(r u_\theta)}{\partial r} + G, \quad (2.2c)$$

where

$$\mathbf{H} = \begin{pmatrix} 0 \\ \nu u_r / r \end{pmatrix}, \quad \mathbf{F} = \begin{pmatrix} r a_x \\ P - 2\nu u_r / r + u_\theta^2 + r a_r \end{pmatrix}, \quad G = r^2 a_\theta.$$

Here $\mathbf{u} = (u_x, u_r)$ is the corresponding velocity in the meridian plane, and $P = p/\rho$, $\nabla = (\partial/\partial x, \partial/\partial r)$. It can be found that the structure of Eqs. (2.2a) and (2.2b) are similar to the standard Navier-Stokes equations. Eq. (2.2c) also can be regarded as an advection-diffusion equation with source terms.

2.2 Incompressible axisymmetric LBGK model

Based on the feature of Eqs. (2.2a) and (2.2b) mentioned above, we designed a new D2Q9 axisymmetric LBGK model from Guo's incompressible LBGK model [10]. In Eq. (2.2b), there are some additional terms compared with the standard NS equations. Therefore an source term $\delta_t F_i$ is inserted into the evolution equation of the distribution function $f_i(\mathbf{x}, t)$, which can be described as

$$f_i(\mathbf{x} + c\mathbf{e}_i \delta_t, t + \delta_t) - f_i(\mathbf{x}, t) = -\frac{1}{\tau} [f_i(\mathbf{x}, t) - f_i^{(eq)}(\mathbf{x}, t)] + \delta_t F_i, \quad (2.3)$$

where $c = \delta_x / \delta_t$, δ_x and δ_t are the lattice spacing and the time step, respectively. τ is the dimensionless relaxation time, and $\mathbf{x} = (x, r)$.

The directions of the discrete velocity of the model are given by

$$\mathbf{e}_i = (e_{ix}, e_{ir}) = \begin{cases} (0, 0), & \text{for } i=0, \\ \left(\cos \left[\frac{(i-1)\pi}{2} \right], \sin \left[\frac{(i-1)\pi}{2} \right] \right), & \text{for } i=1-4, \\ \sqrt{2} \left(\cos \left[\frac{(i-5)\pi}{2} + \frac{\pi}{4} \right], \sin \left[\frac{(i-5)\pi}{2} + \frac{\pi}{4} \right] \right), & \text{for } i=5-8. \end{cases}$$

The local equilibrium distribution function $f_i^{(eq)}$ is defined as

$$f_i^{(eq)} = \begin{cases} r\rho_0 - 4\sigma \frac{Pr}{c^2} + s_0(\mathbf{u}), & \text{for } i=0, \\ \lambda \frac{Pr}{c^2} + s_i(\mathbf{u}), & \text{for } i=1-4, \\ \gamma \frac{Pr}{c^2} + s_i(\mathbf{u}), & \text{for } i=5-8, \end{cases} \quad (2.4)$$

where the constant ρ_0 is the fluid average density, and $s_i(\mathbf{u})$ is given by

$$s_i(\mathbf{u}) = r\omega_i \left[\frac{\mathbf{c}_i \cdot \mathbf{u}}{c_s^2} + \frac{(\mathbf{c}_i \cdot \mathbf{u})^2}{2c_s^4} - \frac{\mathbf{u}^2}{2c_s^2} \right],$$

here $c_s = c/\sqrt{3}$ is the sound speed of the model, and $\mathbf{c}_i = c\mathbf{e}_i$. ω_i is weight coefficient and given by $\omega_0 = 4/9$, $\omega_i = 1/9$ for $i = 1-4$, and $\omega_i = 1/36$ for $i = 5-8$. The parameters σ , λ and γ satisfy the following relations

$$\begin{cases} \lambda + \gamma = \sigma, \\ \lambda + 2\gamma = \frac{1}{2}. \end{cases} \quad (2.5)$$

The term F_i can be written in a power series in the particle velocity [34, 35],

$$F_i = \omega_i \left[A + \frac{\mathbf{B} \cdot \mathbf{c}_i}{c_s^2} + \frac{\mathbf{C} : (\mathbf{c}_i \mathbf{c}_i - c_s^2 \mathbf{I})}{2c_s^4} \right]. \quad (2.6)$$

In order to recover the correct equations (2.2a) and (2.2b), A , \mathbf{B} and \mathbf{C} can be specified through the undetermined coefficient method. The zeroth to second moments of F_i are

$$\sum_{i=0}^8 F_i = A, \quad \sum_{i=0}^8 \mathbf{c}_i F_i = \mathbf{B}, \quad \sum_{i=0}^8 \mathbf{c}_i \mathbf{c}_i F_i = c_s^2 \mathbf{A} \mathbf{I} + \frac{1}{2} [\mathbf{C} + \mathbf{C}^T]. \quad (2.7)$$

The fluid velocity \mathbf{u} and pressure P are given by

$$\mathbf{u} = \frac{1}{r} \left(\sum_{i=0}^8 c\mathbf{e}_i f_i + m\mathbf{F}\delta_t \right), \quad P = \frac{3c^2}{5r} \left[\sum_{i=1}^8 f_i + s_0(\mathbf{u}) \right]. \quad (2.8)$$

Through the Chapman-Enskog expansion, the Eqs. (2.2a) and (2.2b) can be derived from this incompressible LBGK model (see the Appendix for details). The kinematic viscosity is determined by $\nu = (\tau - 0.5)\delta_t c_s^2$. The unknown parameters A , \mathbf{B} , m and \mathbf{C} are given by Eqs. (A.11) and (A.12), respectively

$$A = 0, \quad \mathbf{B} = m \left(2 - \frac{1}{\tau} \right) \mathbf{F}, \quad m = \frac{1}{2}, \quad \mathbf{C} = c_s^2 \left(1 - \frac{1}{2\tau} \right) \begin{pmatrix} 0 & u_x \\ u_x & 2u_r \end{pmatrix}.$$

Since \mathbf{F} is usually a function of velocity \mathbf{u} and pressure P , to determine \mathbf{u} and P at the same time, we solve simultaneous equations of \mathbf{u} and P , and rewrite them as

$$u_x = \frac{1}{r} \sum_{i=0}^8 c e_{ix} f_i + \frac{1}{2} \delta_t a_x, \quad u_r = \frac{-b_2 + \sqrt{b_2^2 - 4b_1 b_3}}{2b_1}, \quad P = \frac{3c^2}{5r} \left[\sum_{i=1}^8 f_i + s_0(\mathbf{u}) \right], \quad (2.9)$$

where

$$b_1 = 0.45r\omega_0\delta_t, \quad b_2 = r^2 + \delta_t\nu, \quad b_3 = b_1 u_x^2 - r \sum_{i=0}^8 c e_{ir} f_i - 0.3c^2\delta_t \sum_{i=1}^8 f_i - 0.5r\delta_t(u_\theta^2 + ra_r).$$

When including the influence of azimuthal rotation, we need to solve Eq. (2.2c), a D2Q4 or D2Q5 LBGK model can be designed for such an advection-diffusion equation. The idea is come from the thermal lattice Bhatnagar-Gross-Krook (TLBGK) model which is proposed for Boussinesq incompressible fluids [33]. However, in order to keep the sound speed c_s consistent with that in the incompressible LBGK model for Eqs. (2.2a) and (2.2b), a D2Q5 LBGK model is adopted for the azimuthal velocity. The evolution equation for Eq. (2.2c) can be expressed as

$$g_i(\mathbf{x} + c\mathbf{e}_i\delta_t, t + \delta_t) - g_i(\mathbf{x}, t) = -\frac{1}{\tilde{\tau}} [g_i(\mathbf{x}, t) - g_i^{(eq)}(\mathbf{x}, t)] + \delta_t G_i, \quad (2.10)$$

g_i ($i = 0-4$) is the distribution function of azimuthal velocity. $\tilde{\tau}$ is also a dimensionless relaxation time. The equilibrium distribution function $g_i^{(eq)}$ and the source term G_i are given as

$$g_i^{(eq)} = r^2 u_\theta \tilde{\omega}_i \left[1 + \frac{c\mathbf{e}_i \cdot \mathbf{u}}{c_s^2} \right], \quad G_i = \tilde{\omega}_i \left[E + \frac{\mathbf{R} \cdot c\mathbf{e}_i}{c_s^2} \right], \quad (2.11)$$

where $\tilde{\omega}_i$ is weight coefficients, and given by $\tilde{\omega}_0 = 1/3$, $\tilde{\omega}_i = 1/6$ for $i = 1-4$. The zeroth and first moments of G_i are

$$\sum_{i=0}^4 G_i = E, \quad \sum_{i=0}^4 c_i G_i = \mathbf{R}. \quad (2.12)$$

The azimuthal velocity u_θ is determined by g_i

$$u_\theta = \frac{1}{r^2} \left(\sum_{i=0}^4 g_i + \frac{\delta_t}{2} G \right) = \frac{1}{r^2} \sum_{i=0}^4 g_i + \frac{\delta_t}{2} a_\theta. \quad (2.13)$$

Through the Chapman-Enskog expansion, the Eq. (2.2c) can be derived from the D2Q5 LBGK model (see the Appendix for details). The kinematic viscosity ν and $\tilde{\tau}$ satisfy such an relational expression $\nu = (\tilde{\tau} - 0.5)\delta_t c_s^2$. It can be found that $\tilde{\tau}$ equal to the dimensional relation time τ in Eq. (2.3). The unknown parameters E and \mathbf{R} are given by Eqs. (A.22) and (A.23), respectively

$$E = \left(1 - \frac{1}{2\tilde{\tau}} \right) G, \quad \mathbf{R} = \begin{pmatrix} 0 \\ 3c_s^2 r u_\theta (1 - 1/(2\tilde{\tau})) \end{pmatrix}.$$

In summary, the present model has some advantages. First, Based on the framework of Guo's incompressible LBGK model [10], the model can properly simulate the incompressible axisymmetric flows only with the small Mach number limit. Second, the terms $-\nu \partial \mathbf{u} / \partial r + \mathbf{H}$ and $-3\nu \partial (r u_\theta) / \partial r$ can be recovered from the source terms which contain no gradients. When simulating the incompressible axisymmetric flows, these features make the implementation of the present model be easier and more accurate.

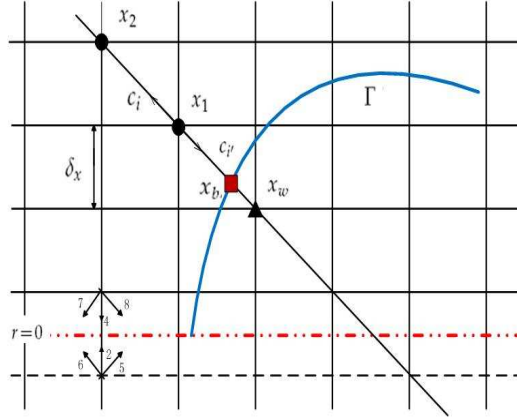


Figure 1: The geometry condition of curved wall boundary.

3 Boundary conditions and force evaluation

To study a problem with LBGK model, the distribution functions at the fluid nodes near the boundary must be specially treated. Nowadays, there have been many boundary conditions treatments for curved boundary [36–38]. In these schemes, Guo’s scheme has better numerical stability compared with the other two treatments [38]. Here we will extend this non-equilibrium extrapolation scheme (NEES) proposed by Guo et al. [31,38] to the present incompressible axisymmetric LBGK model.

In Fig. 1, the link between the fluid node x_1 and the wall node x_w intersects the physical boundary at x_b , and $\mathbf{x}_1 = \mathbf{x}_w + c\mathbf{e}_i\delta_t$, $\Delta = |\mathbf{x}_1 - \mathbf{x}_b| / |\mathbf{x}_1 - \mathbf{x}_w|$. As we know, the evolution equation of the LBGK model consists of two computational steps:

$$\text{collision:} \quad \varphi_i^+(\mathbf{x}, t) - \varphi_i(\mathbf{x}, t) = -\frac{1}{\tau}(\varphi_i(\mathbf{x}, t) - \varphi_i^{(eq)}(\mathbf{x}, t)) + \delta_t S_i, \tag{3.1a}$$

$$\text{streaming:} \quad \varphi_i(\mathbf{x} + c\mathbf{e}_i\delta_t, t + \delta_t) = \varphi_i^+(\mathbf{x}, t), \tag{3.1b}$$

where $\varphi_i = f_i$ or g_i and $S_i = F_i$ or G_i . In order to determine the distribution function $\varphi_i(\mathbf{x}_1, t + \delta_t)$ at the fluid node x_1 , we need to first specify the post-collision distribution function $\varphi_i^+(\mathbf{x}_w, t)$ at the wall node x_w . Based on the idea of the NEES, the distribution function at x_w can be decomposed into its equilibrium and non-equilibrium parts, $\varphi_i(\mathbf{x}_w, t) = \varphi_i^{(eq)}(\mathbf{x}_w, t) + \varphi_i^{(neq)}(\mathbf{x}_w, t)$. The equilibrium part is approximated with the extrapolated velocity and pressure. For the non-equilibrium part, we extrapolate the non-equilibrium parts of the neighboring nodes to approximate it. Then the post-collision distribution function $\varphi_i^+(\mathbf{x}_w, t)$ is obtained as

$$\varphi_i^+(\mathbf{x}_w, t) = \varphi_i^{(eq)}(\mathbf{u}_w, P_w) + \left(1 - \frac{1}{\tau}\right)\varphi_i^{(neq)}(\mathbf{x}_w, t) + \delta_t S_i, \tag{3.2}$$

where $P_w = P(\mathbf{x}_1, t)$. \mathbf{u}_w and $\varphi_i^{(neq)}(\mathbf{x}_w, t)$ are determined by [31]

$$\mathbf{u}_w = \begin{cases} \frac{(3-\Delta)\mathbf{u}(\mathbf{x}_b) + (\Delta^2-1)\mathbf{u}(\mathbf{x}_1) - (1-\Delta)^2\mathbf{u}(\mathbf{x}_2)}{1+\Delta}, & \Delta < 0.75, \\ \frac{\mathbf{u}(\mathbf{x}_b) + (\Delta-1)\mathbf{u}(\mathbf{x}_1)}{\Delta}, & \Delta \geq 0.75, \end{cases} \quad (3.3a)$$

$$\varphi_i^{(neq)}(\mathbf{x}_w, t) = \begin{cases} \Delta\varphi_i^{(neq)}(\mathbf{x}_1, t) + (1-\Delta)\varphi_i^{(neq)}(\mathbf{x}_2, t), & \Delta < 0.75, \\ \varphi_i^{(neq)}(\mathbf{x}_1, t), & \Delta \geq 0.75. \end{cases} \quad (3.3b)$$

However, at the axis of symmetry where $r = 0$, the singularity emerges. In order to deal with the axis of symmetry, we will set the first lattice line at $r = 0.5\delta_x$ and apply the symmetry boundary condition [31] to overcome the difficulty.

As mentioned in [31], the momentum exchange at the wall node x_b which occurs during the interactions between the fluid and the wall, will lead to a force exerting on the wall

$$\tilde{\mathbf{F}}(\mathbf{x}_b, t) = -\rho_0 \frac{c\mathbf{e}_i}{\delta_t} \left[\frac{f_i^+(\mathbf{x}_w, t)}{r_w} + \frac{f_{i'}^+(\mathbf{x}_1, t)}{r_1} \right]. \quad (3.4)$$

Then for an axisymmetric body where the axis lies along the x direction, the total drag force on the wall exerted by the fluid can be determined by

$$\tilde{F}_x = 2\pi \int_{\Gamma} \delta_x r \tilde{\mathbf{F}}_x(\mathbf{x}, t) dl \approx -2\pi\rho_0 \frac{\delta_x^2}{\delta_t} \sum c e_{ix} [f_i^+(\mathbf{x}_w, t) + f_{i'}^+(\mathbf{x}_1, t)], \quad (3.5)$$

where Γ is the body surface in the meridian half-plane.

4 Numerical results

To evaluate the incompressible LBGK model proposed in the above section, numerical tests including the steady Hagen-Poiseuille flow with pressure boundary condition, the unsteady Womersley flow, the external flow over a sphere, and the cylindrical cavity flow are carried out. In the following simulations, the parameters of the LBGK model are taken as $\sigma = 5/12$, $\lambda = 1/3$, and $\gamma = 1/12$. The fluid average density ρ_0 is specified as $\rho_0 = 1.0$. The symmetry boundary condition will be employed to deal with the symmetric axis, while the other boundaries will be treated by the NEES.

4.1 Hagen-Poiseuille flow

The Hagen-Poiseuille flow through a straight pipe driven by a constant pressure gradient is defined in the region $0 \leq x \leq 1.0$ and $0 \leq r \leq R$, where $R = 1.0$ is the radius of the pipe. $r = 0$ is the symmetric axis and the solid wall is located at $r = R$. The initial and boundary

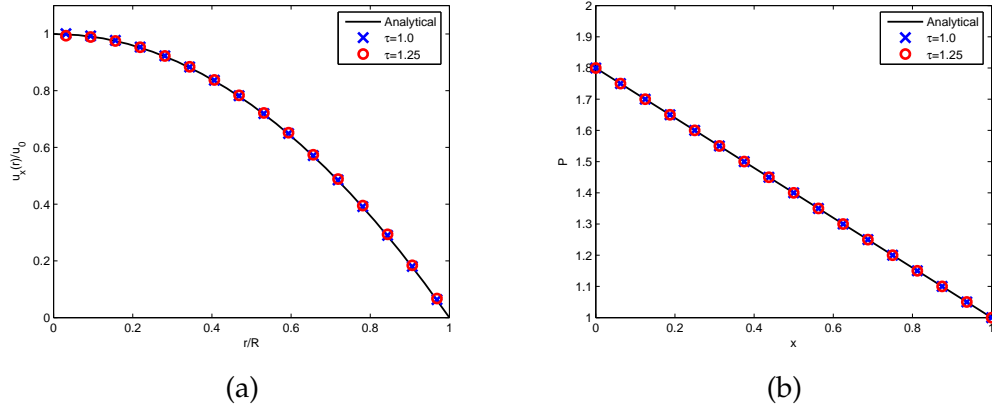


Figure 2: (a) Velocity of the Poiseuille flow ($Re=40$, $\delta_x=R/16$); (b) Pressure of the Poiseuille flow ($Re=40$, $\delta_x=R/16$).

conditions are set as follows,

$$\begin{aligned} u_x(x,r,0) &= u_r(x,r,0) = u_\theta(x,r,0) = 0, & P(x,r,0) &= P_0, \\ u_x(x,R,t) &= u_r(x,R,t) = u_\theta(x,R,t) = 0, \\ P(0,r,t) &= P_{in}, & P(1,r,t) &= P_{out}, \end{aligned}$$

where $P_0 = 0.5(P_{in} + P_{out})$, and P_{in} and P_{out} are the pressure maintained at the entrance and exit, respectively. With these conditions, the problem has an analytic solution,

$$\begin{aligned} u_x(x,r,t) &= u_0 \left(1 - \frac{r^2}{R^2}\right), \\ u_r(x,r,t) &= u_\theta(x,r,t) = 0, \\ P(x,r,t) &= P_{in} - \Delta P x, \end{aligned}$$

where $u_0 = \Delta P R^2 / 4\nu$ is the maximum velocity and $\Delta P = P_{in} - P_{out}$.

In the simulations, the Reynolds number is defined as $Re = 2Ru_0/\nu$. The pressure at the entrance and outlet are initialized to be $P_{in} = 1.8$ and $P_{out} = 1.0$, respectively. The non-equilibrium extrapolation scheme for pressure boundary conditions is applied to the inlet and outlet of the flow, and the NEES is applied to the solid wall. Fig. 2 compares the axial velocity u_x at the mid-width of the pipe $x=0.5$, and the pressure predicted by the present LBGK model with the analytical solution for $Re = 40$. Here a lattice with $\delta_x = R/16$ is used, and two values of the relaxation time, $\tau = 1.0$ and 1.25 , are chosen. As shown in this figure, it is found that the present numerical results are in good agreement with the analytical solutions, and the pressure distribution is linear along the pipe.

The relative global error of u_x with different numbers of lattice nodes in the radius is shown in Fig. 3 where the relative global error is defined as

$$Err(u) = \frac{\|u_x - u_c\|_2}{\|u_c\|_2}, \quad (4.1)$$

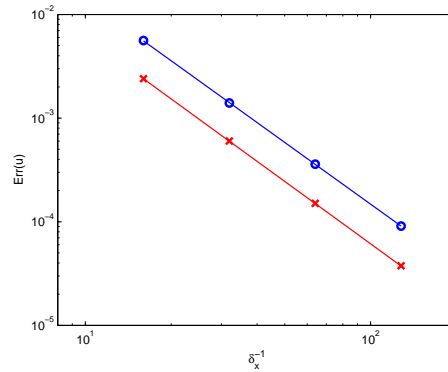


Figure 3: Relative global errors as a function of the lattice spacing δ_x at $Re=40$. \circ : $\tau=1.25$; \times : $\tau=1.0$.

where u_c and u_x are the axial velocities of the analytical solution and numerical results, respectively. The solid lines represent the linear fits, and the slopes of the lines are -2.00 and -1.98 for the cases of $\tau = 1.0$ and $\tau = 1.25$. The results shown in Fig. 3 demonstrate that the current LBGK model is of second order accuracy in space.

In order to demonstrate that the present LBGK model can eliminate the compressible effects, we will study the Hagen-Poiseuille flow using both the present LBGK model and Guo's LBE model [31], and calculate the relative global error in velocity field as a function of the pressure drop, ΔP (or the maximum Mach number $M_{\max} = u_0/c_s$). In the simulations, a lattice with $\delta_x = R/16$ and the relaxation time $\tau = 1.0$ are used, the relative global error is computed by Eq. (4.1). In Table 1, Err_1 is the relative global error derived by using Guo's LBE model, while Err_2 is the error with the present LBGK model. Through the comparison listed in Table 1, it can be found that the errors of the two models are comparable with small pressure drop. That is because density variation $\delta\rho$ is very small such that the error due to compressible effect is almost negligible. As the pressure drop (or the maximum Mach number) increases, the error of Guo's model (Err_1) grows fast, while the error of the present incompressible LBGK model has no change. This is because the variation of pressure will lead to the density variation in Guo's model based on the state equation for perfect gas. On the contrary, as we apply the present axisymmetric LBGK model, in which the macroscopic variables are pressure p and velocity u not density ρ and velocity u , the compressible effect caused by density variation can be reduced. Therefore, compared with Guo's axisymmetric LBE model, the present model can effectively eliminate the compressible effect.

Table 1: The relative global error of velocity field in the Hagen-Poiseuille flow.

ΔP	Re	u_0	M_{\max}	Err_1	Err_2
0.1	5	0.25	0.0451	0.0026	0.0024
0.5	25	1.25	0.2255	0.0215	0.0024
0.8	40	2.0	0.3608	0.0535	0.0024
1.2	60	3.0	0.5413	0.1084	0.0024

4.2 Unsteady Womersley flow

To further test the present LBGK model, the unsteady Womersley flow driven by a oscillatory force with a period T is studied, where $T = 2\pi/\Omega$, and the force $a_x = \tilde{G} \cos(\Omega t)$. Here Ω stands for the frequency of the driven force, and \tilde{G} is the maximum amplitude of the sinusoidally varying force. The geometry of this flow is the same as that of the Hagen-Poiseuille flow. The boundary conditions for the fluid variables are given as follows:

$$\begin{aligned} r=0: \quad & \frac{\partial \varphi}{\partial r} = 0, \quad \forall \varphi, \\ r=R: \quad & u_x = u_r = u_\theta = 0. \end{aligned}$$

The Reynolds number is defined as $2u_0R/\nu$, where the velocity $u_0 = \tilde{G}R^2/4\nu$. The analytical solution of the Womersley flow is

$$u_x(r,t) = Real \left\{ \frac{\tilde{G}}{i\Omega} \left[1 - \frac{J_0(rs/R)}{J_0(s)} \right] e^{i\Omega t} \right\}, \tag{4.2}$$

where R is the radius of the pipe, i is the imaginary unit, and $s = \alpha(i-1)/\sqrt{2}$, α is the Womersley number and defined as $\alpha = R\sqrt{\Omega/\nu}$, J_0 is the zero order bessel function of the first type, and "Real" means the real part of a complex number.

In the simulations, the boundary condition of the top wall is treated by the NEES. In the streamwise direction, periodic boundary conditions are applied to both the inlet and outlet. Initially, the velocity is set to zero everywhere, and all the simulations begin with an initial run of $10T$ steps. Two Womersley numbers, i.e., $\alpha = 8$ and $\alpha = 16$, for $Re = 1200$ are chosen. The numerical results and the analytical solutions for two cases are shown in Fig. 4. As seen from this figure, the numerical results are in good agreement with the analytical ones.

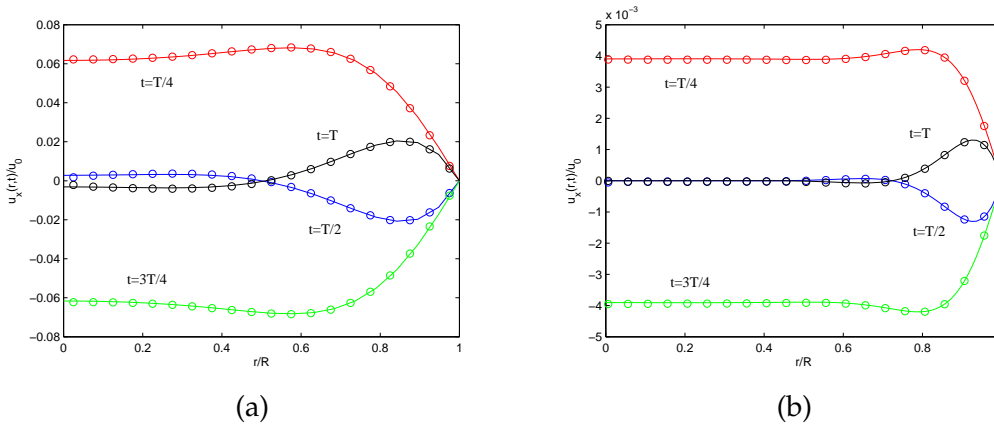


Figure 4: Velocity of the Womersley flow ($Re = 1200$, $\tau = 0.6$). Circle: the numerical results; Solid line: the analytical results. (a) $\alpha = 8$, $\delta_x = R/20$; (b) $\alpha = 16$, $\delta_x = R/80$.

4.3 Flow over a sphere

Experimental and numerical investigations for the external flow over a sphere have been studied by many authors for its widespread applications [39–48]. This problem is also studied and used to demonstrate the capability of the present incompressible LBGK model. The computation domain considered here is $0 \leq x \leq 4R$ and $0 \leq r \leq R$, where $R=0.5$ is the radius of the pipe. $R_s=0.05$ is the radius of the sphere, and the center location of the sphere is $(2R,0)$. The Reynolds number (Re) defined as $2R_s u_0 / \nu$, is varied from 5 to 150, u_0 is the free-stream velocity, and ν is the kinematic viscosity. The boundary conditions of this problem are set as follows,

$$\begin{aligned} \text{The inlet of the flow:} & \quad u_x = u_0, \quad u_r = u_\theta = 0, \\ \text{The outlet of the flow:} & \quad \frac{\partial \psi}{\partial t} + u_0 \frac{\partial \psi}{\partial x} = 0 \quad (\psi = P, u_x, u_r, u_\theta), \\ \text{The side boundaries:} & \quad \frac{\partial \psi}{\partial r} = 0, \\ \text{The surface of the sphere:} & \quad u_x = u_r = u_\theta = 0. \end{aligned}$$

All these boundary conditions are implemented by the NEES. The velocity u_0 is set to be 0.1, the lattice spacing $\delta x = R/160$ is used, and the criterion used for steady state is

$$\frac{\|\mathbf{u}(t) - \mathbf{u}(t - 100\delta t)\|_2}{\|\mathbf{u}(t)\|_2} < 10^{-6}.$$

To compare with previous studies, we have measure the drag force exerted on the sphere. In Fig. 5, the drag coefficients C_d of the present work and previous studies are given, where C_d is calculated by $C_d = 2\tilde{F}_x / \rho_0 \pi u_0^2 R_s^2$. It is clear that the LBGK results agree well with the existing experimental and numerical data.

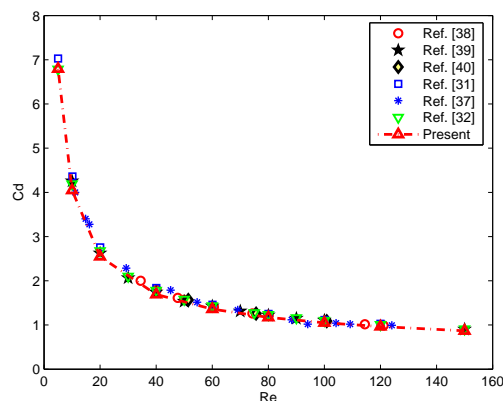


Figure 5: Drag coefficient against the Reynolds number for axisymmetric flow over a sphere.

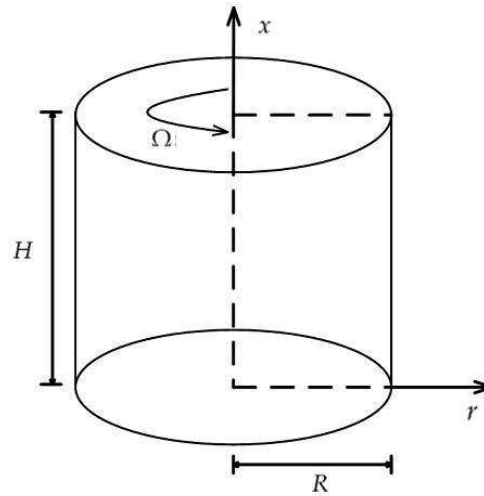


Figure 6: Schematic of the cylindrical cavity flow.

4.4 Cylindrical cavity flow

In the above numerical tests, the azimuthal velocity u_θ equals to zero in the whole computation domain. To further demonstrate the capability of the present LBGK model in simulating the axisymmetric rotational flow, we apply the model to study the rotational flow in a closed cylindrical cavity. The configuration of the problem is shown in Fig. 6. The height and the radius of the cavity are H and R . The bottom of the cavity is closed, whereas the top lid rotates with an angular velocity Ω .

Many numerical and experimental investigations for the cylindrical cavity flow have been studied [13,49–54], in which there are two important dimensionless parameters, i.e., the aspect ratio $A = H/R$ and the rotational Reynolds number $Re = \Omega R^2/\nu$. To consist with the experimental study [54] and the lattice Boltzmann simulations [13,31], we will study this flow with such cases, i.e., (1) $Re = 990$ and $A = 1.5$, (2) $Re = 1290$ and $A = 1.5$, (3) $Re = 1010$ and $A = 2.5$. The simulations are performed with resolution $\delta_x = R/100$. The boundary conditions of the problem are set as follows,

$$\begin{aligned} x=0, \quad 0 \leq r \leq R: \quad u_x = u_r = u_\theta = 0, \\ r=R, \quad 0 \leq x \leq H: \quad u_x = u_r = u_\theta = 0, \\ x=H, \quad 0 \leq r < R: \quad u_x = u_r = 0, \quad u_\theta = \Omega r. \end{aligned}$$

The axis is treated by the symmetry boundary condition, while the NEES is applied to treat the other boundaries. Initially, the velocity at all nodes inside the cavity are taken as zero, and the initial pressure P is set to be 1.0. The obtained streamlines of the cylindrical cavity flow for the three cases are shown in Fig. 7. It can be found that there is not any vortex breakdown revealed for the cases (1) and (3), while for the case (2), a single vortex breakdown appears. These phenomena are consistent with previous experimental and

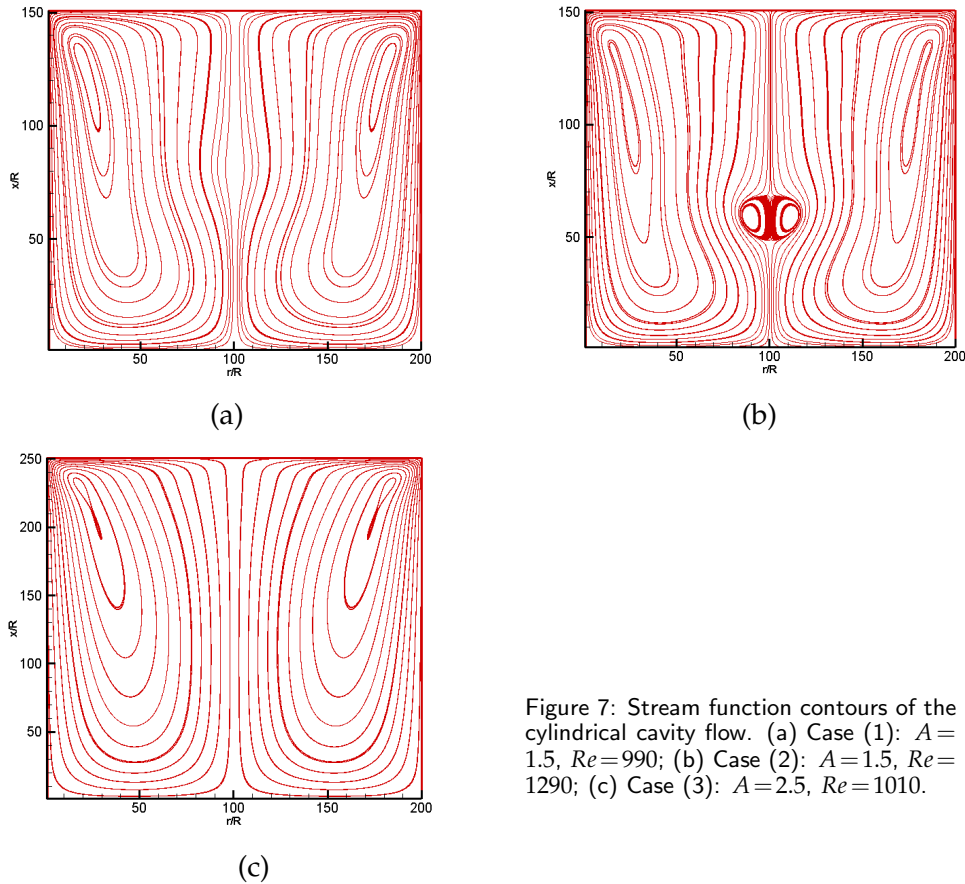


Figure 7: Stream function contours of the cylindrical cavity flow. (a) Case (1): $A = 1.5, Re = 990$; (b) Case (2): $A = 1.5, Re = 1290$; (c) Case (3): $A = 2.5, Re = 1010$.

numerical results [13, 31, 54]. In Fig. 8, the axial velocity u_x on the axis predicted by the present LBGK model are shown and compared with previous results. Here the velocity u_x on the axis is obtained by $u(x,0) = [9u_x(x,0.5\delta_x) - u_x(x,1.5\delta_x)]/8$. From the figure, it is clearly that the present results agree well with the experimental and numerical ones.

5 Summary

In this paper we have proposed a LBGK model for incompressible axisymmetric flows and derived the axisymmetric hydrodynamic equations in the cylindrical coordinate system through the Chapman-Enskog expansion. The compressible effect has been eliminated in the present incompressible LBGK model. The terms $-\nu\partial\mathbf{u}/\partial r + \mathbf{H}$ in the macroscopic momentum equation are recovered by choosing a proper definition of \mathbf{C} to ensure that the source terms of the model contain no velocity gradients.

In order to validate the present LBGK model, we have also performed numerical simulations for several axisymmetric flows. The present LBGK model results agree well with

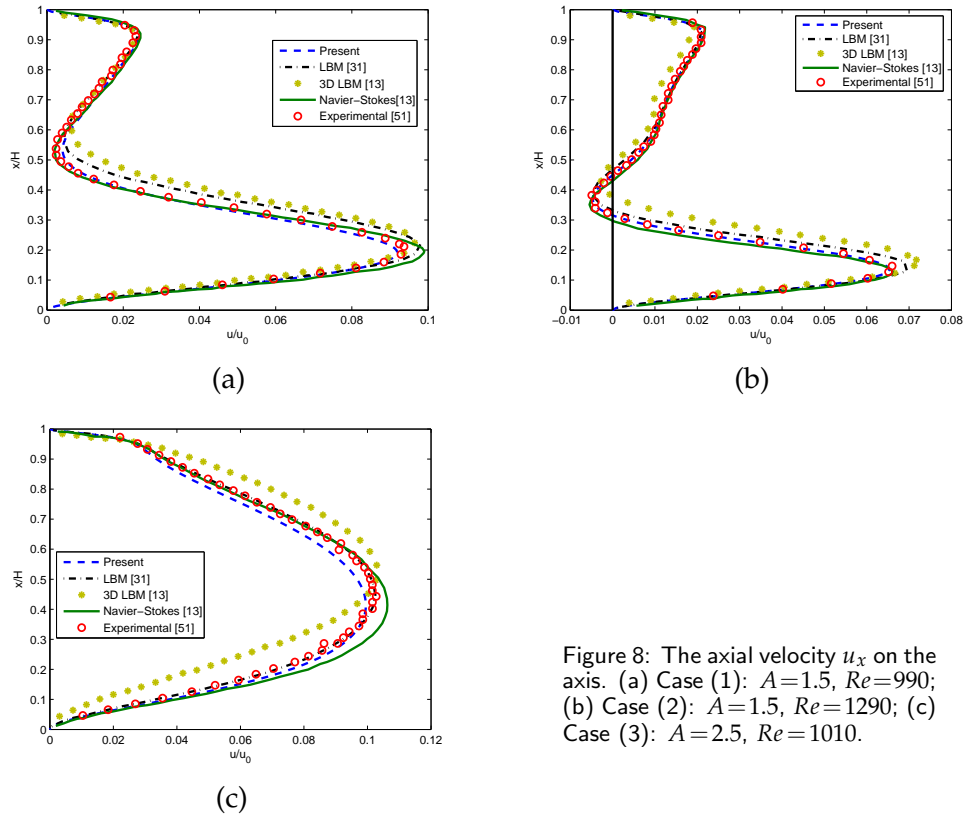


Figure 8: The axial velocity u_x on the axis. (a) Case (1): $A=1.5, Re=990$; (b) Case (2): $A=1.5, Re=1290$; (c) Case (3): $A=2.5, Re=1010$.

the analytical, numerical or experimental data in the literature, which also can be used to specify the capacity of the present model. In addition, compared with previous axisymmetric LBE model, the present model can eliminate the compressible effect only with the small Mach number limit.

Appendix: Champan-Enskog analysis of the incompressible axisymmetric LBGK model

To derive the correct governing equations (2.2a) and (2.2b) for the incompressible axisymmetric flows from the present LBGK model, we first introduce the following expansions by using an expansion parameter ϵ :

$$f_i = f_i^{(0)} + \epsilon f_i^{(1)} + \epsilon^2 f_i^{(2)} + \dots, \tag{A.1a}$$

$$\partial_t = \epsilon \partial_{t1} + \epsilon^2 \partial_{t2}, \quad \nabla = \epsilon \nabla_1, \quad F_i = \epsilon F_i^{(1)}, \tag{A.1b}$$

$$\mathbf{F} = \epsilon \mathbf{F}_1, \quad A = \epsilon A_1, \quad \mathbf{B} = \epsilon \mathbf{B}_1, \quad \mathbf{C} = \epsilon \mathbf{C}_1, \tag{A.1c}$$

where ϵ is proportional to the ratio of the lattice spacing to a characteristic macroscopic length.

Expanding $f_i(\mathbf{x} + \mathbf{c}_i \delta_t, t + \delta_t)$ in Eq. (2.3) about \mathbf{x} and t , and applying the above multiscaling expansions, we can obtain the following equations in consecutive order of the parameter ϵ :

$$\mathcal{O}(\epsilon^0): \quad f_i^{(0)} = f_i^{(eq)}, \tag{A.2a}$$

$$\mathcal{O}(\epsilon^1): \quad D_{1i} f_i^{(0)} = -\frac{1}{\tau \delta_t} f_i^{(1)} + F_i^{(1)}, \tag{A.2b}$$

$$\mathcal{O}(\epsilon^2): \quad \partial_{t_2} f_i^{(0)} + \left(1 - \frac{1}{2\tau}\right) D_{1i} f_i^{(1)} = -\frac{1}{\tau \delta_t} f_i^{(2)} - \frac{\delta_t}{2} D_{1i} F_i^{(1)}, \tag{A.2c}$$

where $D_{1i} = \partial_{t_1} + \mathbf{c}_i \cdot \nabla_1$.

Note that $\mathbf{E}^{(2n+1)} = 0$, for $n = 0, 1, \dots$, where $\mathbf{E}^{(n)}$ are the tensors defined as $\mathbf{E}^{(n)} = \sum_{\alpha} e_{\alpha 1} e_{\alpha 2} \dots e_{\alpha n}$ and

$$\sum_{i=1}^4 e_{i\alpha} e_{i\beta} = 2\delta_{\alpha\beta}, \quad \sum_{i=5}^8 e_{i\alpha} e_{i\beta} = 4\delta_{\alpha\beta}, \tag{A.3a}$$

$$\sum_{i=1}^4 e_{i\alpha} e_{i\beta} e_{i\gamma} e_{i\zeta} = 2\delta_{\alpha\beta\gamma\zeta}, \quad \sum_{i=5}^8 e_{i\alpha} e_{i\beta} e_{i\gamma} e_{i\zeta} = 4\Delta_{\alpha\beta\gamma\zeta} - 8\delta_{\alpha\beta\gamma\zeta}, \tag{A.3b}$$

where $\delta_{\alpha\beta}$ and $\delta_{\alpha\beta\gamma\zeta}$ are the Kronecker tensors, and

$$\Delta_{\alpha\beta\gamma\zeta} = \delta_{\alpha\beta} \delta_{\gamma\zeta} + \delta_{\alpha\gamma} \delta_{\beta\zeta} + \delta_{\alpha\zeta} \delta_{\beta\gamma}. \tag{A.4}$$

With these properties of the $\mathbf{E}^{(n)}$, we can obtain:

$$\sum_i f_i^{(0)} = \rho_0 r, \quad \sum_i \mathbf{c}_i f_i^{(0)} = \mathbf{u} r, \tag{A.5a}$$

$$\sum_i c^2 \mathbf{e}_i \mathbf{e}_i f_i^{(0)} = r \mathbf{u} \mathbf{u} + r P \mathbf{I}, \quad \sum_i f_i^{(m)} = 0, \quad \text{for } m > 0, \tag{A.5b}$$

$$\sum_i \mathbf{c}_i f_i^{(1)} = -m \mathbf{F}_1 \delta_t, \quad \sum_i \mathbf{c}_i f_i^{(m)} = 0, \quad \text{for } m > 1, \tag{A.5c}$$

$$\sum_i c^3 \mathbf{e}_{i\alpha} \mathbf{e}_{i\beta} \mathbf{e}_{i\gamma} f_i^{(0)} = c_s^2 r (\delta_{\alpha\beta} \mathbf{u}_\gamma + \delta_{\alpha\gamma} \mathbf{u}_\beta + \delta_{\gamma\beta} \mathbf{u}_\alpha). \tag{A.5d}$$

With the aids of Eqs. (2.7) and (A.5), from Eq. (A.2b) the equations in moment space at t_1 time scale can be explicitly derived:

$$\nabla_1 \cdot (r \mathbf{u}) = A_1, \quad \partial_{t_1} (r \mathbf{u}) + \nabla_1 \cdot (r \mathbf{u} \mathbf{u} + r P \mathbf{I}) = \frac{m}{\tau} \mathbf{F}_1 + \mathbf{B}_1. \tag{A.6}$$

Similarly, the moments of Eq. (A.2c) lead to the following equations:

$$m\delta_t \left(\frac{1}{2\tau} - 1 \right) \nabla_1 \cdot \mathbf{F}_1 = -\frac{\delta_t}{2} \partial_{t_1} A_1 - \frac{\delta_t}{2} \nabla_1 \cdot \mathbf{B}_1, \tag{A.7a}$$

$$\partial_{t_2} (r\mathbf{u}) - m\delta_t \left(1 - \frac{1}{2\tau} \right) \partial_{t_1} \mathbf{F}_1 + \left(1 - \frac{1}{2\tau} \right) \nabla_1 \cdot \Pi^{(1)} = -\frac{\delta_t}{2} \left(\partial_{t_1} \mathbf{B}_1 + \frac{1}{2} \nabla_1 \cdot (\mathbf{C}_1 + \mathbf{C}_1^T) \right), \tag{A.7b}$$

where $\Pi^{(1)} = \sum_i c^2 \mathbf{e}_i \mathbf{e}_i f_i^{(1)}$ is the first-order momentum flux tensor. With the aid of Eqs. (2.7), (A.2b) and (A.5), we have:

$$\begin{aligned} -\frac{1}{\tau\delta_t} \Pi^{(1)} &= \partial_{t_1} \sum_i c^2 \mathbf{e}_i \mathbf{e}_i f_i^{(0)} + \nabla_1 \cdot \sum_i c^3 \mathbf{e}_i \mathbf{e}_i \mathbf{e}_i f_i^{(0)} - \sum_i c^2 \mathbf{e}_i \mathbf{e}_i \mathbf{F}_i^{(1)} \\ &= \partial_{t_1} (r\mathbf{u}\mathbf{u} + rP\mathbf{I}) + c_s^2 \left[\nabla_1 (r\mathbf{u}) + (\nabla_1 (r\mathbf{u}))^T + (\nabla_1 \cdot (r\mathbf{u}))\mathbf{I} \right] - \frac{1}{2} (\mathbf{C}_1 + \mathbf{C}_1^T) \\ &= c_s^2 \nabla_1 (r\mathbf{u}) + c_s^2 (\nabla_1 (r\mathbf{u}))^T + c_s^2 A_1 \mathbf{I} - \frac{1}{2} (\mathbf{C}_1 + \mathbf{C}_1^T). \end{aligned} \tag{A.8}$$

Note that the terms of $\partial_{t_1} (r\mathbf{u}\mathbf{u} + rP\mathbf{I})$ should be neglected because they are of the order $\mathcal{O}(Ma^2)$, thus

$$\begin{aligned} \left(1 - \frac{1}{2\tau} \right) \nabla_1 \cdot \Pi^{(1)} &= \left(\frac{\delta_t}{2} - \tau\delta_t \right) \nabla_1 \cdot \left[c_s^2 \nabla_1 (r\mathbf{u}) + c_s^2 (\nabla_1 (r\mathbf{u}))^T + c_s^2 A_1 \mathbf{I} - \frac{1}{2} (\mathbf{C}_1 + \mathbf{C}_1^T) \right] \\ &= \left(\frac{\delta_t}{2} - \tau\delta_t \right) c_s^2 \nabla_1 \cdot (\nabla_1 (r\mathbf{u}) + (\nabla_1 (r\mathbf{u}))^T + A_1 \mathbf{I}) - \left(\frac{\delta_t}{4} - \frac{\tau\delta_t}{2} \right) \nabla_1 \cdot (\mathbf{C}_1 + \mathbf{C}_1^T) \\ &= \left(\frac{1}{2} - \tau \right) \delta_t c_s^2 (\nabla_1^2 (r\mathbf{u}) + \nabla_1 A_1) - \left(\frac{\delta_t}{4} - \frac{\tau\delta_t}{2} \right) \nabla_1 \cdot (\mathbf{C}_1 + \mathbf{C}_1^T). \end{aligned} \tag{A.9}$$

We can rewrite the Eq. (A.7b) as:

$$\begin{aligned} \partial_{t_2} (r\mathbf{u}) - m\delta_t \left(1 - \frac{1}{2\tau} \right) \partial_{t_1} \mathbf{F}_1 + \left(\frac{1}{2} - \tau \right) \delta_t c_s^2 (\nabla_1^2 (r\mathbf{u}) + \nabla_1 A_1) + \frac{\tau\delta_t}{2} \nabla_1 \cdot (\mathbf{C}_1 + \mathbf{C}_1^T) \\ = -\frac{\delta_t}{2} \partial_{t_1} \mathbf{B}_1. \end{aligned} \tag{A.10}$$

To recover the correct governing equations (2.2a) and (2.2) for the incompressible axisymmetric flows, the parameters A , \mathbf{B} and m must be chosen as

$$A = 0, \quad \mathbf{B} = m \left(2 - \frac{1}{\tau} \right) \mathbf{F}, \quad m = \frac{1}{2}, \tag{A.11}$$

and a proper definition of \mathbf{C} is given as

$$\mathbf{C} = c_s^2 \left(1 - \frac{1}{2\tau} \right) \begin{pmatrix} 0 & u_x \\ u_x & 2u_r \end{pmatrix}. \tag{A.12}$$

Combining the results on the t_1 and t_2 time scales, Eqs. (A.6) and (A.7) together with Eqs. (A.11) and (A.12), we can obtain the final macroscopic equations accurate to the

order of $\mathcal{O}(\delta_f^2)$ in the continuity equation and $\mathcal{O}(\delta_f^2 + \delta_t Ma^2)$ in the momentum equation:

$$\nabla \cdot (r\mathbf{u}) = 0, \tag{A.13a}$$

$$\frac{\partial(r\mathbf{u})}{\partial t} + \nabla \cdot (r\mathbf{u}\mathbf{u}) = -\nabla(P_r) + \nu \nabla^2(r\mathbf{u}) - \nu \frac{\partial \mathbf{u}}{\partial r} + \mathbf{H} + \mathbf{F}, \tag{A.13b}$$

where the viscosity is

$$\nu = \left(\tau - \frac{1}{2}\right) \delta_t c_s^2. \tag{A.14}$$

Similarly, to recover the governing equation for azimuthal velocity u_θ , i.e., Eq. (2.2c), we introduce the following expansions from the D2Q5 LBGK model,

$$g_i = g_i^{(0)} + \epsilon g_i^{(1)} + \epsilon^2 g_i^{(2)} + \dots, \tag{A.15a}$$

$$\partial_t = \epsilon \partial_{t1} + \epsilon^2 \partial_{t2}, \quad \nabla = \epsilon \nabla_1, \quad G_i = \epsilon G_i^{(1)}, \tag{A.15b}$$

$$G = \epsilon G_1, \quad E = \epsilon E_1, \quad \mathbf{R} = \epsilon \mathbf{R}_1. \tag{A.15c}$$

Through the above expansions, we can obtain the following equations in consecutive order of the parameter ϵ :

$$\mathcal{O}(\epsilon^0): \quad g_i^{(0)} = g_i^{(eq)}, \tag{A.16a}$$

$$\mathcal{O}(\epsilon^1): \quad D_{1i} g_i^{(0)} = -\frac{1}{\tau \delta_t} g_i^{(1)} + G_i^{(1)}, \tag{A.16b}$$

$$\mathcal{O}(\epsilon^2): \quad \partial_{t2} g_i^{(0)} + \left(1 - \frac{1}{2\tau}\right) D_{1i} g_i^{(1)} = -\frac{1}{\tau \delta_t} g_i^{(2)} - \frac{\delta_t}{2} D_{1i} G_i^{(1)}. \tag{A.16c}$$

With the properties of the $\mathbf{E}^{(n)}$, we can find:

$$\sum_{i=0}^4 g_i^{(0)} = r^2 u_\theta, \quad \sum_{i=0}^4 c \mathbf{e}_i g_i^{(0)} = r^2 u_\theta \mathbf{u}, \tag{A.17a}$$

$$\sum_{i=0}^4 c^2 \mathbf{e}_i \mathbf{e}_i g_i^{(0)} = r^2 c_s^2 u_\theta \mathbf{I}, \tag{A.17b}$$

$$\sum_{i=0}^4 g_i^{(1)} = -\frac{\delta_t}{2} G_1, \quad \sum_{i=0}^4 g_i^{(m)} = 0, \quad \text{for } m > 1. \tag{A.17c}$$

With the aids of Eqs. (2.13) and (A.17), we obtain the following equation through summing on i in Eq. (A.16b):

$$\partial_{t1}(r^2 u_\theta) + \nabla_1 \cdot (r^2 u_\theta \mathbf{u}) = \frac{1}{2\tau} G_1 + E_1. \tag{A.18}$$

Similarly, through summing on i in Eq. (A.16c), we obtain:

$$\partial_{t2}(r^2 u_\theta) - \frac{\delta_t}{2} \left(1 - \frac{1}{2\tau}\right) \partial_{t1}(G_1) + \left(1 - \frac{1}{2\tau}\right) \nabla_1 \cdot \Theta^{(1)} = -\frac{\delta_t}{2} (\partial_{t1} E_1 + \nabla_1 \cdot \mathbf{R}_1), \tag{A.19}$$

where $\Theta_{(1)} = \sum_{i=0}^4 c\mathbf{e}_i g_i^{(1)}$. With the aids of Eqs. (2.13), (A.17) and (A.16b), we have

$$\begin{aligned} -\frac{1}{\tilde{\tau}\delta_t}\Theta^{(1)} &= \partial_{t_1} \sum_i c\mathbf{e}_i g_i^{(0)} + \nabla_1 \cdot \sum_i c^2 \mathbf{e}_i \mathbf{e}_i g_i^{(0)} - \sum_i c\mathbf{e}_i G_i^{(1)} \\ &= \partial_{t_1} (r^2 u_\theta \mathbf{u}) + \nabla_1 \cdot (r^2 c_s^2 u_\theta \mathbf{I}) - \mathbf{R}_1 \\ &= \partial_{t_1} (r^2 u_\theta \mathbf{u}) + \nabla_1 (r^2 c_s^2 u_\theta) - \mathbf{R}_1. \end{aligned} \quad (\text{A.20})$$

Note that the term of $\partial_{t_1} (r^2 u_\theta \mathbf{u})$ should be neglected because they are of the order $\mathcal{O}(Ma^2)$, so the Eq. (A.19) can be written as:

$$\partial_{t_2} (r^2 u_\theta) - \frac{\delta_t}{2} \left(1 - \frac{1}{2\tilde{\tau}}\right) \partial_{t_1} (G_1) = \left(\tilde{\tau} - \frac{1}{2}\right) \delta_t c_s^2 \nabla_1^2 (r^2 u_\theta) - \frac{\delta_t}{2} \partial_{t_1} E_1 - \tilde{\tau} \delta_t \nabla_1 \cdot \mathbf{R}_1. \quad (\text{A.21})$$

In order to recover the correct governing equation for u_θ , the parameter E must be chosen as

$$E = \left(1 - \frac{1}{2\tilde{\tau}}\right) G = \left(1 - \frac{1}{2\tilde{\tau}}\right) r^2 a_\theta, \quad (\text{A.22})$$

and a proper definition of \mathbf{R} is given as

$$\mathbf{R} = \begin{pmatrix} 0 \\ 3c_s^2 r u_\theta \left(1 - \frac{1}{2\tilde{\tau}}\right) \end{pmatrix}. \quad (\text{A.23})$$

Combining the results on the t_1 and t_2 time scales, Eqs. (A.18) and (A.21) together with Eqs. (A.22) and (A.23), we can obtain the final macroscopic equation accurate to the order of $\mathcal{O}(\delta_t^2 + \delta_t Ma^2)$:

$$\frac{\partial (r^2 u_\theta)}{\partial t} + \nabla \cdot (r^2 \mathbf{u} u_\theta) = \nu \nabla^2 (r^2 u_\theta) - 3\nu \frac{\partial (r u_\theta)}{\partial r} + G, \quad (\text{A.24})$$

where the viscosity is

$$\nu = \left(\tilde{\tau} - \frac{1}{2}\right) \delta_t c_s^2. \quad (\text{A.25})$$

Acknowledgments

One of authors (T. Zhang) is grateful to Liang Wang for useful discussions. This work is financially supported by the National Basic Research Program of China (Grant No. 2011CB707305), the National Natural Science Foundation of China (Grant Nos. 51006040 and 51006039) and the Fundamental Research Funds for the Central Universities, HUST (Grant Nos. 2010MS131 and 2010JC005).

References

- [1] Y. H. Qian, S. Succi and S. A. Orszag, Recent advances in lattice Boltzmann computing, *Annu. Rev. Comput. Phys.*, 3 (1995), 195–242.
- [2] R. Benzi, S. Succi and M. Vergassola, The lattice Boltzmann equation-theory and applications, *Phys. Rep.*, 222 (1992), 145–197.
- [3] S. Chen and G. D. Doolen, Lattice Boltzmann method for fluid flows, *Annu. Rev. Fluid Mech.*, 30 (1998), 329–364.
- [4] C. K. Aidun and J. R. Clausen, Lattice-Boltzmann method for complex flows, *Annu. Rev. Fluid Mech.*, 42 (2010), 439–472.
- [5] S. Succi, *The Lattice Boltzmann Equation for Fluid Dynamics and Beyond*, Oxford University Press, 2001.
- [6] Q. Zou, S. Hou, S. Chen and G. D. Doolen, An improved incompressible lattice Boltzmann model for time-independent flows, *J. Stat. Phys.*, 81 (1995), 35–48.
- [7] Z. Lin, H. Fang and R. Tao, Improved lattice Boltzmann model for incompressible two-dimensional steady flows, *Phys. Rev. E*, 54 (1997), 6323–6330.
- [8] Y. Chen and H. Ohashi, Lattice-BGK methods for simulating incompressible fluid flows, *Int. J. Mod. Phys. C*, 8 (1997), 793–803.
- [9] X. He and L. S. Luo, Lattice Boltzmann model for the incompressible Navier-Stokes equation, *J. Stat. Phys.*, 88 (1997), 927–944.
- [10] Z. L. Guo, B. C. Shi and N. C. Wang, Lattice BGK model for incompressible Navier-Stokes equation, *J. Comput. Phys.*, 165 (2000), 288–306.
- [11] A. M. Artoli, A. G. Hoekstra and P. M. A. Sloot, 3D pulsatile flow in the lattice Boltzmann BGK method, *Int. J. Mod. Phys. C*, 13 (2002), 1119–1134.
- [12] T. Inamuro, R. Tomita and F. Ogino, Lattice Boltzmann simulations of drop deformation and breakup in shear flows, *Int. J. Mod. Phys. B*, 17 (2003), 21–26.
- [13] S. K. Bhaumik and K. N. Lakshmisha, Lattice Boltzmann simulation of lid-driven swirling flow in confined cylindrical cavity, *Comput. Fluids*, 36 (2007), 1163–1173.
- [14] I. Halliday, L. A. Hammond, C. M. Care, K. Good and A. Stevens, Lattice Boltzmann equation hydrodynamics, *Phys. Rev. E*, 64 (2001), 011208.
- [15] K. N. Premnath and J. Abraham, Lattice Boltzmann model for axisymmetric multiphase flows, *Phys. Rev. E*, 71 (2005), 056706.
- [16] S. Mukherjee and J. Abraham, Lattice Boltzmann simulations of two-phase flow with high density ratio in axially symmetric geometry, *Phys. Rev. E*, 75 (2007), 026701.
- [17] T. S. Lee, H. Huang and C. Shu, An axisymmetric incompressible lattice Boltzmann model for pipe flow, *Int. J. Mod. Phys. C*, 17 (2006), 645–661.
- [18] T. Reis and T. N. Phillips, Modified lattice Boltzmann model for axisymmetric flows, *Phys. Rev. E*, 75 (2007), 056703.
- [19] T. Reis and T. N. Phillips, Numerical validation of a consistent axisymmetric lattice Boltzmann model, *Phys. Rev. E*, 77 (2008), 026703.
- [20] J. G. Zhou, Axisymmetric lattice Boltzmann method, *Phys. Rev. E*, 78 (2008), 036701.
- [21] S. Chen, J. Tölke, S. Geller and M. Krafczyk, Lattice Boltzmann model for incompressible axisymmetric flows, *Phys. Rev. E*, 78 (2008), 046703.
- [22] Y. Peng, C. Shu, Y. T. Chew and J. Qiu, Numerical investigation of flows in Czochralski crystal growth by an axisymmetric lattice Boltzmann method, *J. Comput. Phys.*, 186 (2003), 295–307.
- [23] X. D. Niu, C. Shu and Y. T. Chew, An axisymmetric lattice Boltzmann model for simulation

- of Taylor-Couette flows between two concentric cylinders, *Int. J. Mod. Phys. C*, 14 (2003), 785–796.
- [24] M. E. McCracken and J. Abraham, Simulations of liquid break up with an axisymmetric, multiple relaxation time, index-function lattice Boltzmann model, *Int. J. Mod. Phys. C*, 16 (2005), 1671–1692.
- [25] T. S. Lee, H. Huang and C. Shu, An axisymmetric incompressible lattice BGK model for simulation of the pulsatile flow in a circular pipe, *Int. J. Numer. Meth. Fluids*, 49 (2005), 99–116.
- [26] H. Huang, T. S. Lee and C. Shu, Hybrid lattice Boltzmann finite difference simulation of axisymmetric swirling and rotating flows, *Int. J. Numer. Methods Fluids*, 53 (2007), 1707–1726.
- [27] H. Huang, T. S. Lee and C. Shu, Lattice Boltzmann simulation of gas slip flow in long microtubes, *Int. J. Numer. Meth. Heat Fluid Flow*, 17 (2007), 587–607.
- [28] S. Mukherjee and J. Abraham, Investigations of drop impact on dry walls with a lattice-Boltzmann model, *J. Colloid Interface Sci.*, 312 (2007), 341–354.
- [29] S. Mukherjee and J. Abraham, Crown behavior in drop impact on wet walls, *Phys. Fluids*, 19 (2007), 052103.
- [30] S. Chen, J. Tölke, S. Geller and M. Krafczyk, Simulation of buoyancy-driven flows in a vertical cylinder using a simple lattice Boltzmann model, *Phys. Rev. E*, 79 (2009), 016704.
- [31] Z. L. Guo, H. F. Han, B. C. Shi and C. G. Zheng, Theory of the lattice Boltzmann equation: lattice Boltzmann model for axisymmetric flows, *Phys. Rev. E*, 79 (2009), 046708.
- [32] L. Wang, Z. L. Guo and C. G. Zheng, Multi-relaxation-time lattice Boltzmann model for axisymmetric flows, *Comput. Fluids*, 39 (2010), 1542–1548.
- [33] Z. L. Guo, B. C. Shi and C. G. Zheng, A coupled lattice BGK model for the Boussinesq equations, *Int. J. Numer. Meth. Fluids*, 39 (2002), 325–342.
- [34] A. J. C. Ladd and R. Verberg, Lattice-Boltzmann simulations of particle-fluid suspensions, *J. Stat. Phys.*, 104 (2001), 1191–1251.
- [35] Z. L. Guo, C. G. Zheng and B. C. Shi, Discrete lattice effects on the forcing term in the lattice Boltzmann method, *Phys. Rev. E*, 65 (2002), 046308.
- [36] O. Filippova and D. Hänel, Grid refinement for lattice-BDK models, *J. Comput. Phys.*, 147 (1998), 219–228.
- [37] R. Mei, L. S. Luo and W. Shyy, An accurate curved boundary treatment in the lattice Boltzmann method, *J. Comput. Phys.*, 155 (1999), 307–330.
- [38] Z. L. Guo, C. G. Zheng and B. C. Shi, An extrapolation method for boundary conditions in lattice Boltzmann method, *Phys. Fluids*, 14 (2002), 2007–2010.
- [39] Y. Rimon and S. I. Cheng, Numerical solution of a uniform flow over a sphere at intermediate Reynolds number, *Phys. Fluids*, 12 (1969), 949–959.
- [40] F. W. Roos and W. W. Willmarth, Some experimental results on sphere and disk drag, *AIAA J.*, 9 (1971), 285–291.
- [41] R. Clift, R. J. Grace and E. W. Weber, *Bubbles, Drops and Particles*, Academic Press, New York, 1978.
- [42] S. Shirayama, Flow past a sphere: topological transitions of the vorticity field, *AIAA J.*, 30 (1992), 349–358.
- [43] R. Mittal, A Fourier Chebyshev spectral collocation method for simulation flow past sphere and spheroids, *Int. J. Numer. Methods Fluids*, 30 (1999), 921–937.
- [44] T. A. Johnson and V. C. Patel, Flow past a sphere up to a Reynolds number of 300, *J. Fluid Mech.*, 378 (1999), 19–70.

- [45] X. Y. Wang, K. S. Yeo, C. S. Chew and B. C. Khoo, A SVD-GFD scheme for computing 3D incompressible viscous fluid flows, *Comput. Fluids*, 37 (2008), 733–746.
- [46] J. Kim, D. Kim and H. Choi, An immersed-boundary finite-volume method for simulations of flow in complex geometries, *J. Comput. Phys.*, 171 (2001), 132–150.
- [47] D. Kim and H. Choi, Characteristics of laminar flow past a sphere in uniform shear, *Phys. Fluids*, 17 (2005), 103602.
- [48] R. W. Mei, W. Shyy, D. Z. Yu and L. S. Luo, Lattice Boltzmann method for 3-D flows with curved boundary, *J. Comput. Phys.*, 161 (2000), 680–699.
- [49] M. P. Escudier, Observations of the flow produced in a cylindrical container by a rotating endwall, *Exp. Fluids*, 2 (1984), 189–196.
- [50] H. J. Lugt and H. J. Haussling, Axisymmetric vortex breakdown in rotating fluid within a container, *J. Appl. Mech.*, 49 (1982), 921–923.
- [51] H. J. Lugt and M. Abboud, Axisymmetric vortex breakdown with and without temperature effects in a container with a rotating lid, *J. Fluid Mech.*, 179 (1987), 179–200.
- [52] J. M. Lopez, Axisymmetric vortex breakdown part 1: confined swirling flow, *J. Fluid Mech.*, 221 (1990), 533–552.
- [53] G. L. Brown and J. M. Lopez, Axisymmetric vortex breakdown part 2: physical mechanisms, *J. Fluid Mech.*, 221 (1990), 553–576.
- [54] K. Fujimura, H. S. Koyama and J. M. Hyun, Time-dependent vortex breakdown in a cylinder with a rotating lid, *Trans. ASME. J. Fluids Eng.*, 119 (1997), 450–453.